

Differential cross sections for excitation of H_2 by low-energy electron impact

L R Hargreaves¹ , S Bhari¹, B Adjari¹, X Liu² , R Laher³, M Zammit⁴,
J S Savage⁵, D V Fursa⁵ , I Bray⁵  and M A Khakoo¹

¹ Department of Physics, California State University, Fullerton, CA 92834, United States of America

² Planetary and Space Science Division, Space Environment Technologies, 1676 Palisades Drive, Pacific Palisades, CA, 90272, United States of America

³ Mail Code 100-22, Caltech, 1200E California Blvd, Pasadena, CA 91125, United States of America

⁴ Theoretical Division, Los Alamos National Laboratory, Los Alamos, NM 87545, United States of America

⁵ Curtin Institute for Computation and Department of Physics, Astronomy and Medical Radiation Sciences, Curtin University, Perth, Western Australia 6102, Australia

E-mail: lhargreaves@fullerton.edu

Received 15 June 2017, revised 11 September 2017

Accepted for publication 2 October 2017

Published 31 October 2017



Abstract

Experimental and theoretical differential cross sections (DCS) for the electron-impact excitation of molecular hydrogen to the $B\ ^1\Sigma_u^+$, $c\ ^3\Pi_u$, $a\ ^3\Sigma_g^+$, $C\ ^1\Pi_u$, and the $E(F)\ ^1\Sigma_g^+$ states are presented at incident energies near to threshold. The experimental DCSs were taken at incident energies of 14, 15, 16 and 17.5 eV and for scattering angles from 10° to 130° . The theoretical DCSs are from the convergent close-coupling method which has recently successfully modeled differential electron scattering from H_2 when compared with available experiment at energies of 17.5 eV and above.

Keywords: electron scattering, excitation, differential cross section

(Some figures may appear in colour only in the online journal)

1. Introduction

Molecular hydrogen, H_2 , is both the simplest and most abundant molecule in the Universe. It is important as the most fundamental target in electron–molecule collisions, as well as for modeling of astrophysical phenomena such as planetary and stellar atmospheres, interstellar medium and plasma modeling is without doubt. H_2 also plays a significant role in the environments of highly ionized plasmas as a reducing agent and in fuel cells, and technological environments such as gas and laser discharges, or in technological plasmas used for fusion reactors or fabrication of silicon devices. Accurate electron collision data for H_2 , particularly for excitation and ionization processes, is critical as data inputs for chemical models of technological plasmas and for interpreting spectroscopic data from astrophysical observatories.

There are several measurements of electron impact on H_2 regarding the excitation of the dissociative $b\ ^3\Sigma_u^+$ state, at incident electron energies, E_0 , ranging from near-threshold to

several hundred eV [1–6]. Excitation of this anti-bonding state leads to dissociated H atoms which dominate the chemistry of H_2 plasmas, and which is also enhanced by collisions of ground state H_2 molecules with electron excited $\text{H}\ 2\ ^2S_{1/2}$ metastable atoms. Experimental studies of the valence bound states viz the $B\ ^1\Sigma_u^+$, $c\ ^3\Pi_u$, $a\ ^3\Sigma_g^+$, $C\ ^1\Pi_u$ have been extensive since decay of the $B\ ^1\Sigma_u^+$ and the $C\ ^1\Pi_u$ states to the ground $X\ ^1\Sigma_g^+$ state gives rise to the well-known Lyman and Werner VUV bands. On the other hand the $a\ ^3\Sigma_g^+$ state, which is spin-forbidden and also violates dipole selection rules ($g \leftrightarrow u$ and $+$ \leftrightarrow $-$) to the ground $X\ ^1\Sigma_g^+$ state, radiates to the $b\ ^3\Sigma_u^+$ state resulting in another pathway for producing dissociated H atoms.

In the excitation energy loss spectrum of H_2 , a significant complication is the heavy overlap of the vibrational features for the $B\ ^1\Sigma_u^+$, $c\ ^3\Pi_u$, $a\ ^3\Sigma_g^+$, $C\ ^1\Pi_u$ and $E(F)\ ^1\Sigma_g^+$ electronic states, which is within the resolution of typical high-resolution electron spectrometers. This challenges the analysis of electron energy loss spectra (EELS), by requiring the EELS to

be unfolded into its electronic components. Given these constraints, DCS measurements for these states have been reported for excitation of the $B\ ^1\Sigma_u^+$ ($v' = 2$) feature by Srivastava and Jensen [7], which is spectrally isolated. Khakoo and Trajmar [8] made an unfolding analysis based on the method of Cartwright *et al* [9] using single Gaussians to simulate the instrumental line profile for E_0 of 20–60 eV. Improved analysis using multi-Gaussian line profiles of the instrumental function was carried out on spectra from a more sophisticated spectrometer by Wrkich *et al* [10] for E_0 of 17.5, 20 and 30 eV. In addition to electronic excitation, at the total (or integral) cross section level, measurements exist for all major processes, including elastic scattering and momentum transfer, ionization, rotational and vibrational excitation, dissociation and dissociative attachment, with these measurements summarized in several review articles [11–14]. The most recent review article of Yoon *et al* [11] (as well as others) offered recommended integrated cross section (ICS) data for H_2 collisions for all such processes.

In addition to the applied importance of this target, H_2 is sufficiently simple that its wave functions are known accurately, and thus provides an ideal target for testing the collisional dynamics of an electron–molecule scattering theory. A number of theoretical studies have considered the problem of electron– H_2 scattering. However, at present no single theoretical solution for electron scattering from any molecule (including H_2) is available in the literature that performs adequately across all scattering processes and incident energies required for modeling purposes. Indeed, the cross sections recommended by Yoon *et al* were essentially entirely from measurements that, in many cases, excluded all available theory. The most advanced theoretical approaches have included the Schwinger variational method approach [15, 16], the complex Kohn approach [17], the *R*-matrix approach [18–22] and the time-dependent close-coupling approach [23]. Recently, Zammit *et al* [24] reported their extension of the convergent close-coupling (CCC) approach, traditionally noted for its treatment of electron scattering from one- and two-electron atoms, to H_2 and reported both differential and integral excitation and ionization cross sections (as well as elastic scattering and total cross sections) at energies from threshold up to 300 eV. The CCC results showed remarkably consistent agreement with available experimental DCS, as compared with other models.

Presently, the lowest incident energy data for excitation is the 17.5 eV result of Wrkich *et al* [10] and the 15 eV data of Srivastava and Jensen [7], restricted to the $B\ ^1\Sigma_u^+$ $v' = 2$ level only. At low E_0 values nuclear dynamics are expected to increase in importance from a physical point of view and must be incorporated for both experiment (in the experimental data analysis, viz breakdown of the Franck–Condon principle) and theory, especially increased in resonant conditions in the formation of negative ion complexes [25]. From the point of view of theory, as the incident energy is reduced away from the ionization threshold the number of open channels reduces and channel coupling effects become less important and progressively easier to handle as the scattering matrix becomes smaller (a problem whose solution is primarily

related to the availability of computational resources and numerical stability), allowing even more focused consideration on the description of the scattering dynamics. In this paper, we report both measurements and CCC calculations of excitation cross sections for the $B\ ^1\Sigma_u^+$, $c\ ^3\Pi_u$, $a\ ^3\Sigma_g^+$, $C\ ^1\Pi_u$ and $E(F)\ ^1\Sigma_g^+$ bound states of H_2 . The current data extend the earlier measurements of Wrkich *et al* to energies as low as 14 eV, and thus are the lowest energy data (for the bound states of H_2) currently available.

2. Experimental details

2.1. Apparatus

The apparatus used for the present measurements has been described extensively in prior publications (e.g. [26, 27]). As a result, here we report only the most salient aspects of the experiment. The experiment consisted of an energy-selected electron gun, producing a well-collimated electron beam. This electron beam intersected a beam of H_2 , formed by the effusive flow of hydrogen gas through a 0.3 mm diameter aperture of 0.025 mm thickness, located 6 mm below the electron beam axis. Electrons scattered from the overlapping volume of these two beams entered an electron analyzer, where they were filtered according to their energy. Those electrons that passed through the filter impacted onto a discrete dynode electron detector, whose output was amplified and conditioned by standard pulse shaping electronics, before being registered by a counter/timer installed into a data acquisition PC. The entire experiment was housed in a stainless steel, high vacuum chamber that ran at a base pressure of 1×10^{-7} Torr, or 4×10^{-6} Torr when gas was admitted into the system. The vacuum tank was lined with a dual layer μ metal shield, which reduced the penetration of magnetic fields into the experiment. The vertical component of the residual magnetic field was further annulled by a single Helmholtz coil mounted to outside of the vacuum chamber. In combination, the magnetic field at the interaction region was less than 5 milli-gauss in any direction, and less than 1 milli-gauss in the direction of the coils (vertical).

The electron gun and analyzer were essentially identical in design. Both used titanium electrostatic lenses, of cylindrical geometry, to transport and focus electrons produced by thermionic emission from a thoriated tungsten filament onto the gas beam, and then focus scattered electrons onto the detector. Molybdenum apertures were installed in both devices to define the incident and scattered electron volumes. Both featured double hemispherical electron energy selectors that controlled the energy spread of the electron beam (in the case of the electron gun), and scattered electrons (in the case of the analyzer). The energy range of the present measurements was 14 eV up to 17.5 eV, with the beam energy calibrated against the well-known He $2\ ^2S$ resonance at 19.36 eV. The total energy resolution of the system (including contributions from the gun and analyzer) was about 70 meV, full-width-at-half-maximum. The analyzer was mounted onto a turntable such that it could be located at any scattering angle

(θ) up to around 130° , beyond which the analyzer and gun would collide. Measurements in the vicinity of 0° were also precluded due to interference from the primary electron beam, limiting the smallest scattering angle at which measurements were possible to approximately 10° , depending on the E_0 under study. The view cone of the analyzer was approximately $\pm 2.5^\circ$. The gun and analyzer were both heated by magnetic-field free biaxial resistive heaters to minimize surface contaminants and ensure the long term stability of the apparatus.

This electron beam intersected the gas source at right angles. The collimated gas source was mounted into a moveable source arrangement as described by Hughes *et al* [28], wherein the gas beam could be either directed into the electron beam, or rotated away to make background measurements. This setup allows backgrounds to be expediently and accurately measured by quickly switching between signal and background measurements every few minutes without any interruption in data sequencing. Data was typically acquired for approximately 4–8 h at each E_0 and θ incident energy and angle (including both background and signal measurements), with each data point repeated at least once (or multiple times, if warranted) as a consistency check.

2.2. Data acquisition and analysis

EELS were obtained by repetitively ramping the analyzer's acceptance energy over H_2 's elastic and inelastic features. A typical spectrum is shown in figure 1. Several peaks are clearly visible, which arise due to excitation of the vibrationally allowed modes of the various electronically excited states. As there is significant overlap between the vibrational energy loss features, the measured spectra must be unfolded to obtain discrete state-to-state cross sections. This unfolding was done by fitting a single profile to the spectrum for each electronic transition present, at each measured E_0 and θ . The fitting routine was a weighted, linear least squares fitting routine, constrained for non-negativity using the active-set routine of Bro and de Jong [29].

The functional form of each electronic transition profile ($S(E_0, \theta, \Delta E)$) was given as:

$$S(E_0, \theta, \Delta E) = C \sum_n \sum_{v'} q_{n,v'} \frac{k_f}{k_0} F(\Delta E - \Delta E_{n,v'}), \quad (1)$$

where $q_{n,v'}$ represents the Franck–Condon factors (FCF) for the transition to the v' th vibrational level of the n th electronic state, $F(\Delta E - \Delta E_{n,v'})$ represents a normalized instrument line function (with ΔE the electron energy loss), k_f and k_0 are the final and initial electron momenta (k_f/k_0 itself represents a velocity ratio ‘scattering flux factor’) and C is the normalization constant determined by the fitting routine, subject to the constraint that $C \geq 0$. The line function of the instrument generally exhibits some deviation from a simple Gaussian profile, primarily observed as rotational broadening of the peaks, and so was modeled by fitting a multi-Gaussian

function to the elastic feature in the EELS, written as:

$$F(\Delta E - \Delta E_{n',v}) = \sum_m \frac{A_m}{\Delta_m \sqrt{\pi}} \times \exp\left(-\left(\frac{\Delta E - \Delta E_{n',v} - \Delta E_m}{\Delta_m}\right)^2\right). \quad (2)$$

In addition, the fitting software allowed for the energy per bin value (the ratio of the total energy loss range scanned and the number of points) to be nonlinearly optimized in order to minimize the final χ^2 value of the fit, although in general this value varied by less than 5%.

The success of this fitting routine depends principally on two factors. The first is the availability of spectroscopic studies to identify the vertical excitation energy ($\Delta E_{n',v}$) of each vibrational line. The second is the availability of FCFs, which specify the relative intensity of each vibration within a given transition based on the Franck–Condon principle. In principle, the spectrum can be fitted without recourse to the FCFs, simply fitting each vibration as an individual line. However, this is ill-advised as the number of free parameters in the model increases by an order of magnitude. As we have discussed in prior publications [27], fitting a large numbers of free parameters, particularly where the states are overlapped, is susceptible to issues due to non-uniqueness. This can result in derived cross sections which, although consistent with the measured spectra, are unphysical and tend to be unstable with even small adjustments to the parameters of the model or assumptions about the experimental conditions. The FCFs and excitation energies assumed in this work are listed in table 1, and a description of the procedure to determine them is given in the next section.

In addition to the bound states, the present EELS also contains a contribution from the dissociative $b^3\Sigma_u^+$ state, which persists to energy losses of about 13 eV. This state was included by modeling the distribution of the state according to the description given in Khakoo and Segura [6], and fitting this profile to the EELS as an additional state. As the overwhelming majority of the state lies outside of our measured energy loss region however, we do not present any DCS data derived from this fitting here to represent the whole continuum. An example of a fitted EELS is shown in figure 1.

Once the data had been unfolded, absolute values for the DCS were determined by computing the ratio of the area of each inelastic feature to that of the elastic peak and multiplying this value by the value of the elastic DCS, taken from the most recent measurements of Muse *et al* [30]. These data are compared with elastic results from the present CCC calculations, shown in figure 2 at two selected incident energies. The agreement between the CCC results and the measurements is clearly excellent at both energies, giving us confidence in the reliability of the DCS used for calibration.

In comparing the elastic to inelastic features in the EELS, it is important to recognize that the focusing and transmission of the analyzer varies with scattered electron energy, and hence the analyzer's transmission efficiency is certainly not constant as the acceptance energy is ramped from the elastic

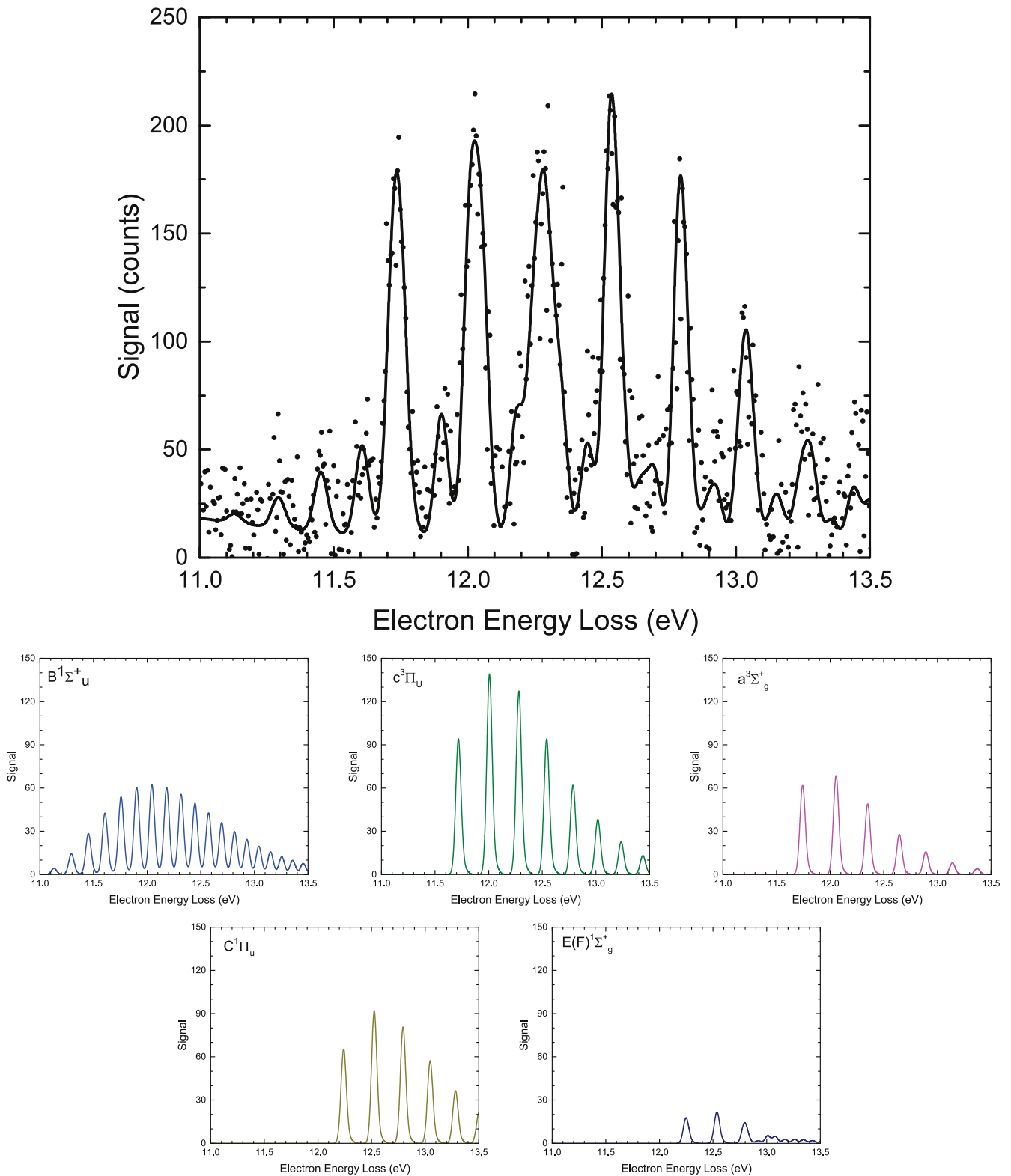


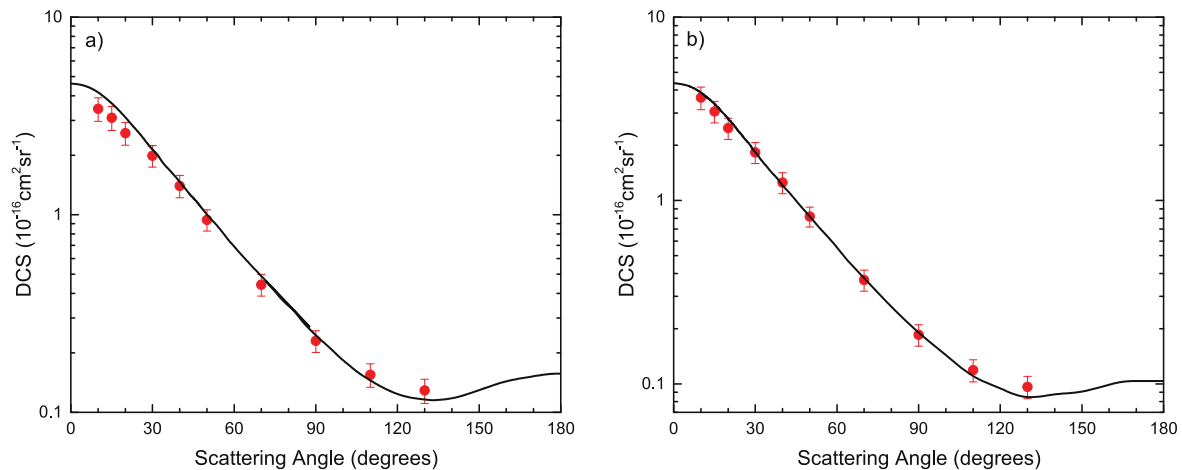
Figure 1. Examples of a fitted EELS, here acquired at an incident energy of 15 eV and scattering angle of 40° . Shown below the fitted EELS are the unfolded component profiles for the five lowest energy states, although note that all energetically open states are included in the fit.

to inelastic features. We characterized this transmission curve by measuring EELS for N_2 at a single scattering angle (90°) for each energy considered. This spectrum was then compared to the equivalent data of LeClair and Trajmar [31], who measured EELS for N_2 using a time-of-flight type energy

analyzer for the scattered electrons. Since such an analyzer uses no focusing fields, their measured spectra are free from transmission variations at different scattered electron energies. A comparison of their data with our own N_2 measurements under equivalent kinematics thus yields the

Table 1. Excitation energies and Frank–Condon factors for excitation of the $X^1\Sigma_g^+$ ($v'' = 0$) to the $B(v')$, $a(v')$, $C(v')$ and $E(F)(v')$ transitions in H_2 , obtained from [54] and in the course of the present study.

v'	$B^1\Sigma_u^+$		$c^3\Pi_u$		$a^3\Sigma_g^+$		$C^1\Pi_u$		$E(F)^1\Sigma_g^+$	
	$\Delta E_{v',0}$ (eV)	FCF	$\Delta E_{v',0}$ (eV)	FCF	$\Delta E_{v',0}$ (eV)	FCF	$\Delta E_{v',0}$ (eV)	FCF	$\Delta E_{v',0}$ (eV)	FCF
0	11.1724	0.00401	11.7594	0.11387	11.7844	0.20437	12.2817	0.12008	12.2877	0.12214
1	11.3353	0.01428	12.0489	0.18587	12.0966	0.25310	12.5669	0.19013	12.3018	0.03548
2	11.4937	0.02951	12.3233	0.18851	12.3920	0.20231	12.8356	0.18828	12.3978	0.00000
3	11.6478	0.04635	12.5829	0.15498	12.6871	0.13013	13.0884	0.15204	12.5759	0.16637
4	11.7978	0.06138	12.8283	0.11415	12.9340	0.08309	13.3245	0.11059	12.5873	0.04904
5	11.9437	0.07235	13.0594	0.07915	13.1811	0.04913	13.5447	0.07609	12.7213	0.00071
6	12.0857	0.07844	13.2767	0.05313	13.4125	0.02867	13.7486	0.05089	12.8295	0.11688
7	12.2236	0.07990	13.4797	0.03513	13.6280	0.01675	13.9363	0.03363	12.8561	0.06242
8	12.3577	0.07762	13.6686	0.02313	13.8273	0.00988	14.1077	0.02215	12.9662	0.02017
9	12.4879	0.07270	13.8432	0.01526	14.0097	0.00591	14.2603	0.01461	13.0520	0.06450
10	12.6145	0.06619	14.0032	0.01013	14.1739	0.00359	14.3939	0.00962	13.1221	0.05833
11	12.7371	0.05893	14.1479	0.00678	14.3183	0.00220	14.5063	0.00625	13.2133	0.03704
12	12.8564	0.05157	14.2764	0.00456	14.4399	0.00134	14.5944	0.00384	13.3028	0.03855
13	12.9717	0.04452	14.3878	0.00307	14.5348	0.00078	14.6594	0.00161	13.3861	0.03753
14	13.0832	0.03804	14.4805	0.00205	14.5984	0.00039			13.4714	0.02979
15	13.1921	0.03224	14.5538	0.00131	14.6306	0.00014			13.5581	0.02424
16	13.2970	0.02716	14.6050	0.00075	14.6411	0.00005			13.6414	0.02128
17	13.3990	0.02279	14.6349	0.00035	14.6470	0.00004			13.7195	0.01848
18	13.4972	0.01906	14.6482	0.00013	14.6514	0.00002			13.7896	0.01532
19	13.5927	0.01591	14.6537	0.00004	14.6542	0.00001			13.8819	0.01252
20	13.6845	0.01327	14.6571	0.00001					13.9561	0.01039
21	13.7739	0.01106							14.0355	0.00876
22	13.8592	0.00923							14.0994	0.00737
23	13.9424	0.00770							14.1793	0.00614
24	14.0216	0.00643							14.2430	0.00509
25	14.0976	0.00538							14.3086	0.00421
26	14.1715	0.00450							14.3645	0.00349

**Figure 2.** DCS for elastic scattering of electrons by H_2 at incident energies of (a) 15 and (b) 17.5 eV. Indicated in the figures are the measurements of Muse *et al* (red circles) [30] and theoretical results from the present CCC calculations employing a 491-state model (black solid curve).

transmission response curve of the analyzer, which can be used to remove transmission effects from our own data.

ICS data were also determined from the present data by integrating the DCS over all angles from 0° to 180° and applying the standard integral. Since the analyzer cannot cover the full angular range, missing data at small and large

angles were recovered from an extrapolation procedure, where the distribution of CCC results (scaled where the calculation differed in magnitude from the measurements) were used as a guide to extrapolate the measurements into the unmeasured angular regions. Uncertainties on the measured DCS data include contributions from statistical uncertainties

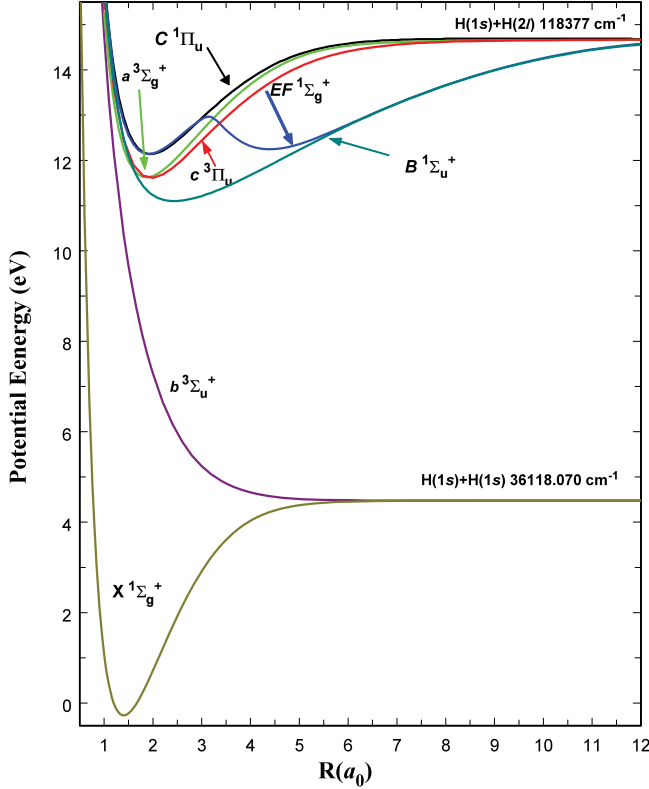


Figure 3. Potential energy curves of the H_2 $X^1\Sigma_g^+$, $b^3\Sigma_u^+$, $a^3\Sigma_g^+$, $c^3\Pi_u$, $B^1\Sigma_u^+$, $C^1\Pi_u^+$ and $E(F)^1\Sigma_g^+$ states. All are based on the *ab initio* calculations of by [37–39, 41]. All energy values are relative to the $v = 0$ and $J = 0$ level of the $X^1\Sigma_g^+$ state. Numerical values in cm^{-1} refer to appropriate asymptotic limits. The asymptotic limits of the $a^3\Sigma_g^+$, $c^3\Pi_u$, $B^1\Sigma_u^+$ and $C^1\Pi_u^+$ states are $\text{H}(1s) + \text{H}(2p)$ while that of the $E(F)^1\Sigma_g^+$ state is $\text{H}(1s) + \text{H}(2s)$. For this reason, less precise values are given to the $\text{H}(1s) + \text{H}(2\ell)$.

(3%–5%) and the uncertainty of the H_2 elastic DCS (around 15%, as quoted by Muse *et al* [30]), summed in quadrature. The statistical uncertainty also includes a term due to the unfolding (taken from the covariance matrix of the fit), however, it should be noted that the assumption of Franck–Condon behavior greatly constrains the fit model and the covariance between the various parameters is very small. It should be noted here that the error due to the unfolding is primarily limited by the accuracy of the Franck–Condon approximation, which is difficult to meaningfully quantify. For the ICS data an additional uncertainty is included to account for the extrapolation by computing the difference between the extrapolated DCS and a ‘flat extrapolated’ DCS (the DCS at the endpoints are assumed to be equal to the nearest measured value). As the integration includes a $\sin(\theta)$ weighting, which heavily weights out the contribution to the ICS from the unmeasured angular regions, the difference between the assumed extrapolation and the flat-extrapolation is generally around 2%.

2.2.1. Determination of Franck–Condon factors and excitation energies. The FCF, by definition, is the square of the overlap of the vibrational wave functions of the initial and

Table 2. Two-electron energies E , vertical excitation energies ΔE , and oscillator strengths f (length) for the electronic target states of H_2 at the internuclear distance $R = 1.448 a_0$ and compared with the sum of vibrationally resolved oscillator strengths from [55].

State	E (a.u.)	ΔE (eV)	f	[55]
$X^1\Sigma_g^+$	−1.161			
$a^3\Sigma_g^+$	−0.715	12.14		
$c^3\Pi_u$	−0.707	12.36		
$B^1\Sigma_u^+$	−0.704	12.45	0.288	0.274
$E(F)^1\Sigma_g^+$	−0.693	12.73		
$C^1\Pi_u$	−0.693	12.83	0.342	0.355

final states involved in the excitation. The potential curves for the present FCF determinations are plotted in figure 3. Both FCF and $\Delta E_{n,v'}$ are traditionally calculated from wave functions and energies of two rotationless levels. However, each observed EEL peak is actually composed of many ro-vibronic excitations and each excitation has different threshold energy. Furthermore, the vibrational wave function implicitly depends of the rotational quantum, J , via the centrifugal potential. For light molecule such as H_2 and its isotopes, the J -dependence of the vibrational overlap integral and $\Delta E_{n,v'}$ can be significant. To fully account for the J -dependence, the present analysis used the effective FCF and $\Delta E_{n,v'}$ that are the sums of individual square of vibrational overlap integral and transition energy weighted by their normalized relative contribution to the EELS peak.

Based on the work of Liu *et al* [32, 33], the cross section of a $|X, v, J\rangle \rightarrow |n, v', J'\rangle$ excitation can be expressed as a product of an electronic form factor, the square of vibrational overlap integral ($|\langle v, J | v', J' \rangle|^2$) and an appropriate rotational factor (or a sum of rotational factors). The rotational factor for different electronic excitations of H_2 have been given in Liu *et al* [32–36]. The electronic form factor, which accounts for magnitude and excitation energy dependence of the cross section, can be considered as a common factor for a given electronic excitation at a given energy. Therefore, the contribution of each $|X, 0, J\rangle \rightarrow |n, v', J'\rangle$ excitation to the effective or weighted FCF equals to the product of the $|\langle v = 0, J | v', J' \rangle|^2$, rotational factor, and the fraction of H_2 population of the $|X, 0, J\rangle$ level at room temperature (300 K). The population fraction are calculated exactly from measured $X^1\Sigma_g^+(v, J)$ energies.

The vibrational overlap integral, $|\langle v, J | v', J' \rangle|^2$, is explicitly evaluated from the vibrational wave functions, which are, in turn, obtained from numerical solution of nuclear Schrödinger equation. For the $E(F)^1\Sigma_g^+$ state, the Born–Oppenheimer (BO) potential and adiabatic correction of Orlowski *et al* [37] were used. For all other states, the BO potentials and adiabatic corrections of Wolniewicz [38], Staszewska and Wolniewicz [39–41], along with appropriate relativistic and radiative corrections, were used. The construction of the singlet-ungerade and triplet potentials has been described by Liu *et al* [33, 36, 42]. In the absence of the non-adiabatic correction, the obtained vibrational wave

Table 3. Measured DCS and ICS data at 17.5 eV for the five lowest excited states of H₂. Units for the DCS data are 10⁻¹⁸ cm² sr⁻¹. Units for the ICS data are 10⁻¹⁸ cm².

$\theta(^{\circ})$	$B\ ^1\Sigma_u^+$		$c\ ^3\Pi_u$		$a\ ^3\Sigma_g^+$		$C\ ^1\Pi_u$		$E(F)\ ^1\Sigma_g^+$	
	DCS	Error	DCS	Error	DCS	Error	DCS	Error	DCS	Error
10	11.323	1.706	2.293	0.346	1.701	0.257	9.393	1.415	1.782	0.269
15	8.251	1.243	2.040	0.308	1.399	0.211	7.636	1.151	0.888	0.134
20	5.233	0.789	1.539	0.232	1.141	0.172	5.295	0.798	0.392	0.059
25	3.779	0.570	1.474	0.222	1.008	0.152	3.973	0.599	0.182	0.028
30	2.908	0.439	1.517	0.229	0.807	0.122	3.086	0.466	0.156	0.024
40	1.868	0.283	1.405	0.213	0.479	0.073	1.672	0.253	0.110	0.017
50	1.388	0.210	1.171	0.177	0.258	0.039	1.220	0.185	0.081	0.012
60	1.357	0.206	1.045	0.158	0.238	0.036	1.058	0.160	0.051	0.008
70	1.245	0.189	0.905	0.137	0.141	0.022	0.740	0.112	0.054	0.008
80	1.395	0.212	0.894	0.136	0.099	0.015	0.404	0.062	0.161	0.025
90	1.091	0.143	0.699	0.114	0.209	0.045	0.251	0.018	0.219	0.039
100	0.807	0.123	0.842	0.137	0.267	0.058	0.354	0.054	0.235	0.042
110	0.583	0.089	0.974	0.150	0.191	0.029	0.292	0.045	0.197	0.030
120	0.362	0.056	1.030	0.158	0.220	0.033	0.389	0.060	0.267	0.041
130	0.246	0.038	1.108	0.170	0.237	0.037	0.498	0.077	0.248	0.038
ICS	16.040	2.410	13.000	2.050	4.520	1.010	12.960	1.900	2.810	0.500

Table 4. Measured DCS and ICS data at 16 eV for the five lowest excited states of H₂. Units for the DCS data are 10⁻¹⁸ cm² sr⁻¹. Units for the ICS data are 10⁻¹⁸ cm².

$\theta(^{\circ})$	$B\ ^1\Sigma_u^+$		$c\ ^3\Pi_u$		$a\ ^3\Sigma_g^+$		$C\ ^1\Pi_u$		$E(F)\ ^1\Sigma_g^+$	
	DCS	Error	DCS	Error	DCS	Error	DCS	Error	DCS	Error
10	4.983	0.751	1.486	0.224	1.524	0.230	2.462	0.371	0.742	0.112
15	4.414	0.665	1.803	0.272	1.512	0.228	2.099	0.317	0.684	0.103
20	3.228	0.486	1.531	0.231	1.079	0.163	2.169	0.327	0.289	0.044
25	2.431	0.366	1.294	0.195	1.014	0.153	1.826	0.275	0.190	0.029
30	1.949	0.294	1.294	0.195	0.786	0.119	1.455	0.219	0.098	0.015
40	1.266	0.191	0.981	0.148	0.600	0.091	0.911	0.138	0.099	0.015
50	1.080	0.164	0.946	0.143	0.287	0.044	0.653	0.099	0.065	0.010
60	0.999	0.152	0.765	0.117	0.195	0.031	0.435	0.067	0.098	0.015
70	0.963	0.146	0.585	0.089	0.240	0.037	0.301	0.046	0.097	0.015
80	1.027	0.156	0.602	0.091	0.268	0.041	0.213	0.032	0.117	0.018
90	0.934	0.141	0.595	0.090	0.328	0.050	0.162	0.025	0.129	0.020
100	1.063	0.165	0.911	0.141	0.231	0.038	0.114	0.020	0.133	0.021
110	0.856	0.131	0.888	0.136	0.152	0.024	0.116	0.018	0.167	0.025
120	0.671	0.102	1.016	0.155	0.103	0.016	0.116	0.018	0.185	0.028
130	0.464	0.071	0.980	0.150	0.208	0.032	0.174	0.027	0.222	0.034
ICS	12.670	1.930	10.700	1.670	4.480	0.750	5.440	0.840	2.370	0.470

function $|v, J\rangle$ can be considered as exact. The difference between the calculated and measured energies of the $C\ ^1\Pi_u^-$, $c\ ^3\Pi_u^-$ and $d\ ^3\Pi_u^-$ states are mainly due to the non-adiabatic correction, which are always less than 2 cm⁻¹. To further increase the accuracy of the transition energies, the measured energies of the $X\ ^1\Sigma_g^+$ state by Dabrowski [43], the $B\ ^1\Sigma_u^+$ and $C\ ^1\Pi_u^+$ states by Abgrall *et al* [44–46] and Roncin and Launay [47], the (corrected) $E(F)\ ^1\Sigma_g^+$, $a\ ^3\Sigma_g^+$, $c\ ^3\Pi_u$ and $e\ ^3\Sigma_u^+$ states of Dieke (as tabulated by Crosswhite [48]) were used to calculate ro-vibronic transition frequencies. The non-adiabatic energies of the $a\ ^3\Sigma_g^+$ state by Wolniewicz [49] are also used when the measured energies were not available. The errors in

the tabulated FCF and $\Delta E_{n,v'}$ are expected to be less than 0.8% and 2 cm⁻¹ (~ 0.2 meV), respectively.

3. Theoretical details

Recently the molecular CCC method [50] has been applied to electron scattering from H₂ [24, 51]. This approach is formulated in a single-center coordinate system and applies the BO approximation to the total scattering wave function. The scattering calculations are then performed within the fixed-nuclei approximation [52]. In the CCC approach the total

Table 5. Measured DCS and ICS data at 15 eV for the five lowest excited states of H₂. Units for the DCS data are 10⁻¹⁸ cm² sr⁻¹. Units for the ICS data are 10⁻¹⁸ cm².

$\theta(^{\circ})$	$B \ ^1\Sigma_u^+$		$c \ ^3\Pi_u$		$a \ ^3\Sigma_g^+$		$C \ ^1\Pi_u$		$E(F) \ ^1\Sigma_g^+$	
	DCS	Error	DCS	Error	DCS	Error	DCS	Error	DCS	Error
10	2.679	0.404	1.437	0.217	0.919	0.139	1.044	0.157	0.896	0.135
15	2.346	0.353	1.658	0.250	0.842	0.127	1.352	0.204	0.533	0.080
20	1.732	0.261	1.414	0.213	0.791	0.119	1.095	0.165	0.506	0.076
25	1.422	0.215	1.434	0.217	0.633	0.096	1.152	0.174	0.237	0.036
30	1.205	0.182	1.319	0.200	0.551	0.084	0.989	0.150	0.141	0.022
40	0.892	0.135	1.099	0.167	0.331	0.051	0.730	0.111	0.081	0.013
50	0.681	0.103	0.871	0.132	0.184	0.029	0.470	0.072	0.100	0.016
60	0.718	0.109	0.672	0.102	0.156	0.024	0.331	0.051	0.118	0.019
70	0.706	0.107	0.538	0.082	0.214	0.033	0.233	0.036	0.158	0.024
80	0.864	0.131	0.586	0.089	0.311	0.047	0.191	0.029	0.211	0.032
90	0.756	0.113	0.588	0.084	0.358	0.067	0.105	0.011	0.242	0.037
100	0.758	0.116	0.818	0.117	0.358	0.067	0.092	0.015	0.303	0.046
110	0.665	0.102	0.969	0.148	0.238	0.037	0.134	0.021	0.259	0.040
120	0.512	0.079	1.163	0.180	0.143	0.023	0.290	0.045	0.244	0.038
130	0.387	0.060	1.132	0.174	0.194	0.030	0.322	0.050	0.289	0.045
ICS	9.030	1.370	11.030	1.700	3.930	0.680	4.520	0.700	3.370	0.640

Table 6. Measured DCS and ICS data at 14 eV for the five lowest excited states of H₂. Units for the DCS data are 10⁻¹⁸ cm² sr⁻¹. Units for the ICS data are 10⁻¹⁸ cm².

$\theta(^{\circ})$	$B \ ^1\Sigma_u^+$		$c \ ^3\Pi_u$		$a \ ^3\Sigma_g^+$		$C \ ^1\Pi_u$		$E(F) \ ^1\Sigma_g^+$	
	DCS	Error	DCS	Error	DCS	Error	DCS	Error	DCS	Error
15	0.954	0.147	0.723	0.112	0.552	0.086	0.370	0.058	0.124	0.020
20	0.811	0.127	0.638	0.100	0.462	0.073	0.318	0.051	0.132	0.022
25	0.660	0.104	0.753	0.118	0.402	0.064	0.312	0.050	0.097	0.016
30	0.570	0.089	0.695	0.108	0.345	0.054	0.265	0.042	0.076	0.012
40	0.438	0.069	0.598	0.093	0.265	0.042	0.278	0.044	0.046	0.008
50	0.364	0.058	0.424	0.067	0.133	0.022	0.142	0.023	0.027	0.005
60	0.336	0.053	0.271	0.043	0.152	0.025	0.092	0.015	0.042	0.007
70	0.452	0.071	0.301	0.048	0.258	0.041	0.110	0.018	0.074	0.012
80	0.528	0.083	0.417	0.066	0.335	0.053	0.082	0.014	0.103	0.017
90	0.582	0.087	0.537	0.084	0.404	0.067	0.105	0.016	0.139	0.037
100	0.657	0.102	0.844	0.131	0.354	0.058	0.117	0.019	0.154	0.025
110	0.580	0.091	0.961	0.149	0.281	0.044	0.124	0.020	0.116	0.019
120	0.568	0.089	1.046	0.162	0.182	0.029	0.159	0.026	0.146	0.023
130	0.474	0.074	0.920	0.143	0.196	0.031	0.185	0.030	0.111	0.018
ICS	6.370	1.000	8.150	1.290	3.590	0.600	2.130	0.370	1.660	0.540

scattering wave function is expanded over the target molecular electronic pseudostates and a set of close-coupling equations are formulated for the scattering T -matrix elements. By performing a partial-wave expansion of the projectile wave functions, the close-coupling equations can be solved for each total symmetry (\mathcal{M} , Π , \mathcal{S}) of the scattering system, where \mathcal{M} is the total orbital angular momentum projection, Π is the total parity, and \mathcal{S} is the total electronic spin. Integrated and differential cross sections are calculated utilizing standard orientation averaging techniques and the higher partial waves are accounted for using a Born top-up procedure [51].

In the CCC calculations H₂ electronic target states are constructed from a diagonalization procedure of the target

electronic Hamiltonian in a set of antisymmetrized two-electron configurations, which are constructed from a Sturmian (Laguerre) basis. As the size of the Laguerre basis increases, the negative-energy states (relative to the H₂⁺ ground state) converge to true bound states and the positive-energy states provide an increasingly dense representation of the target continuum, which allows us to treat all electronically driven reaction channels (including ionization). The CCC calculations rely on the underlying Laguerre basis properties in order to establish convergence of the scattering calculations, which is essentially done by increasing the size of the basis. For near-threshold excitations and/or relatively small scattering cross sections we must also consider the numerical stability of

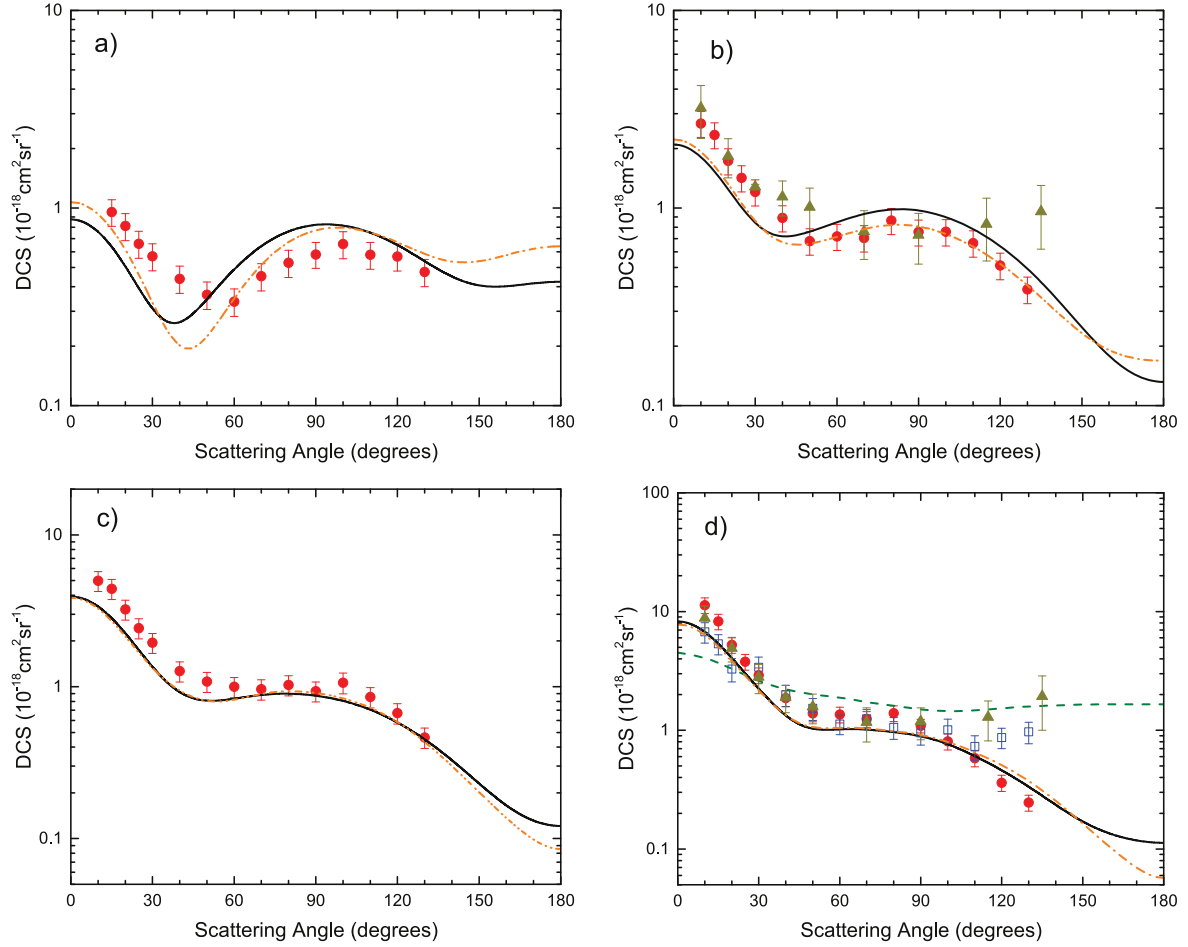


Figure 4. DCS for excitation of the $X^1\Sigma_g^+ \rightarrow B^1\Sigma_u^+$ transition in H_2 at incident energies of (a) 14, (b) 15, (c) 16 and (d) 17.5 eV. Indicated in the figures are the present data (red circles), measurements of Wrkich *et al* (blue open squares) and of Srivistava and Jensen [7] (dark yellow triangles) and theoretical results from the present CCC calculations at the 491-state model (black solid curve) and 427-state model (orange dash-dot curve), and SMC data from da Costa *et al* [15] (green dashed curve).

the scattering calculations. Here we test the convergence and numerical stability of the CCC calculations by comparing two models, a 491- and 427-state model (where degenerate states $m_T = \pm|m_T|$ are counted separately) at the fixed-internuclear separation $R = 1.448 a_0$, which is the average internuclear distance of the H_2 ground state.

The CCC(491) model (491 states) utilizes an underlying Laguerre basis constructed from $N_l = 17 - l$ functions for $l \leq 3$, where N_l is the number of Laguerre basis functions for a given orbital angular momentum l . This model resulted in 92 bound states of H_2 and 399 continuum pseudostates. To check convergence with respect to the number of Laguerre basis functions N_l we have performed scattering calculations with the CCC(427) model, which differs from the CCC(491) model only by the size of the Laguerre basis, $N_l = 15 - l$. These models largely differ in the discretization of the target continuum. Good agreement between the two calculations would indicate convergence of the obtained collision data with respect to the discretization of the target continuum and give a good indication of the numerical stability of the calculations.

The accuracy of the target state wave function also plays an important role in the establishment of reliable cross

sections. In table 2 we present vertical excitation energies and length gauge oscillator strengths for transitions from the electronic ground state at the mean internuclear separation of the ground state $R = 1.448 a_0$. Previously [51] we have shown that these two models obtain converged results for the major scattering cross sections and we estimated the uncertainty of the electron-impact excitation ICSs to be approximately 11% within the fixed-nuclei approximation. The majority of the uncertainty arises from the accuracy of the target wave functions. It is important to note that in the fixed-nuclei approximation and orientation averaging procedure (used in the CCC calculations to calculate cross sections [24, 51]) the closure-method is utilized to analytically sum over all final rovibrational transitions.

4. Results and discussion

Our experimental DCS and ICS results are tabulated in tables 3, 4, 5 and 6. The experimental and theoretical DCS results are compared to each other in figure 4 as well as existing experiment and theoretical models for the excitation of the $B^1\Sigma_u^+$ state. Similarly, the DCS are shown in figure 5

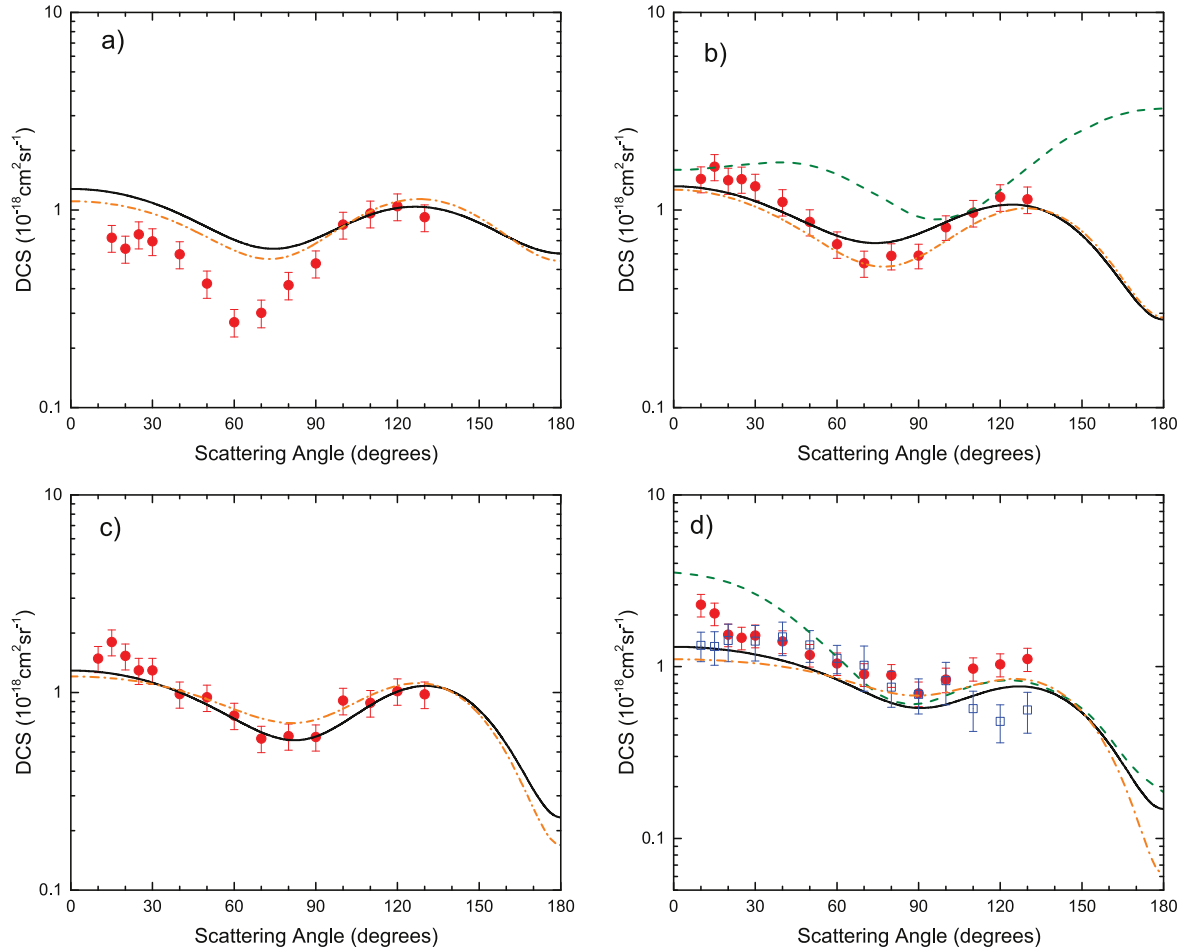


Figure 5. DCS for excitation of the $X^1\Sigma_g^+ \rightarrow c^3\Pi_u$ transition in H_2 at incident energies of (a) 14, (b) 15, (c) 16 and (d) 17.5 eV. Symbols are per figure 4.

for the $c^3\Pi_u$ state, figure 6 for the $a^3\Sigma_g^+$ state, figure 7 for the $C^1\Pi_u$ and figure 8 for the $E(F)^1\Sigma_g^+$. In figure 9, the summed DCS of these five transitions are shown, in order to remove the unfolding procedure as a parameter from the experimental data. In figure 10, ICS are presented for the excitation of these states derived from integrating the DCS as aforementioned.

In figure 4(d), for excitation of the $B^1\Sigma_u^+$ state at $E_0 = 17.5$ eV, good agreement is observed with our earlier DCSs of Wrkich *et al* [10] and with the CCC results. In particular, we note that the present measurements agree with the CCC results particularly well at $\theta > 100^\circ$, showing a downward distribution, whereas the data of Wrkich *et al* hint at a backward peak. At $\theta \leq 30^\circ$ the CCC results match the results of Wrkich *et al* [10] better than the present measurements, which are higher by about 50%. At the E_0 values of 15 and 16 eV (figures 4(c) and (b)), this trend continues i.e. that the present values show higher forward scattering than the CCC results. This is not likely to be due to a forward alignment problem in the experiment, as the disagreement begins quite early in θ at 30° as compared to the angular resolution. The $B^1\Sigma_u^+$ state is the most isolated spectrally from the rest of the H_2 spectrum, and so we expect this state to be the most accurate for which we can determine the DCSs. Also shown are the SMC results of da Costa *et al* [15] at 17.5 eV. The

SMC shows a much flatter distribution compared with any available measurement or the CCC results.

Also shown are the $B^1\Sigma_u^+$ DCSs of Jensen and Srivastava [7]. As they only gave DCS results for the $v' = 2$ line of the $B^1\Sigma_u^+$ state, we have scaled their data according to the FCF distributions used in the present study (modified by the appropriate flux factor at each incident energy), in order to compare with their data. The applied scaling factors were 22.9, 28.7, 31.1, 31.7, 32.1 and 32.3 at their measured incident energies of 15, 20, 30, 40, 50 and 60 eV, respectively. To compare with our data at the highest incident energy of 17.5 eV, which Srivastava and Jensen did not explicitly measure, we have averaged their results at 15 and 20 eV. The agreement with their DCSs at 15 eV is excellent at scattering angles up to 100° , also suggesting a larger forward peak than the CCC results. At larger scattering angles, the data of Srivastava and Jensen shows a backward peak at both incident energies considered, not observed in either the present experiments or theory. At $E_0 = 17.5$ eV, their data supports a smaller DCS at forward angles than suggested by the present measurements, in agreement with the CCC and measurements of Wrkich *et al*.

At the lowest E_0 of 14 eV, (figure 4(a)) the agreement between the experiment and CCC results is qualitatively good

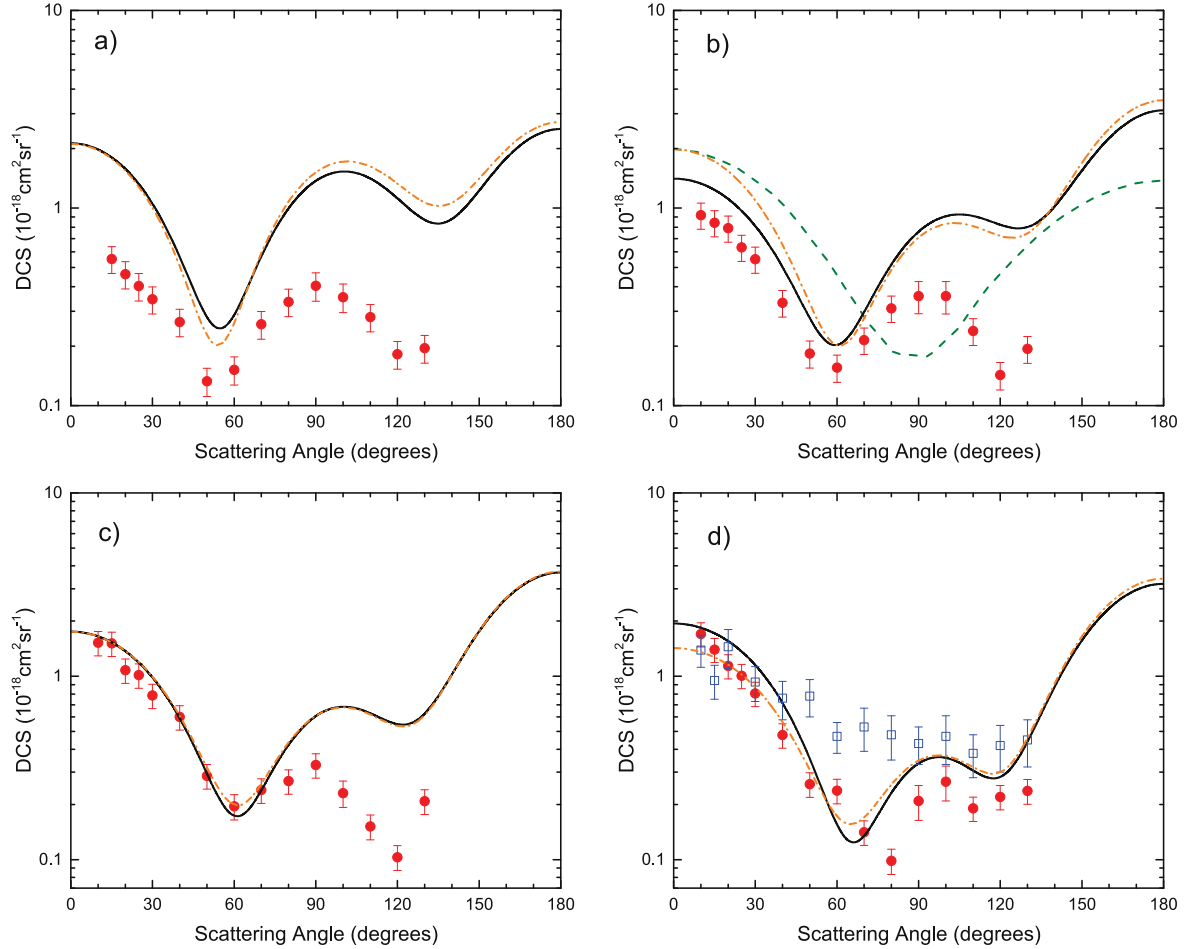


Figure 6. DCS for excitation of the $X^1\Sigma_g^+ \rightarrow a^3\Sigma_g^+$ transition in H_2 at incident energies of (a) 14, (b) 15, (c) 16 and (d) 17.5 eV. Symbols are per figure 4.

for the $B^1\Sigma_u^+$ state, showing similar angular distributions, but differing in the extent of the maxima in these distributions. The large difference in the $\theta \leq 60^\circ$ DCSs may indicate the role of nuclear dynamics at these low energies, which are expected to be most significant at the lowest energies and not included in the fixed-nuclei approximation employed by the CCC method, especially as the rotational quantum energy of H_2 is the largest for any diatomic. In the ground state the spacing between $J = 0$ and $J = 1$ is 15.1 meV, with $\Delta J = 1$ increasing almost linearly with the higher value transitions as J increases, which indicates a significant role of nuclear motion in the excitation scattering dynamics.

For another dipole allowed transition viz. the $C^1\Pi_u$ state (figure 7) we observe similar raised forward scattering at $E_0 = 17.5$ eV (figure 7(d)) compared with the data of Wrkich *et al* [10], whereas the two experiments agree very well at $\theta > 40^\circ$. The CCC results support the larger forward angle DCS seen in the present measurement, and also shows the backward scattering distribution observed in both experiments. The exception is that as the energy is lowered, a shoulder becomes apparent in the CCC results at around $\theta = 80^\circ$, which is not observed in the measurements. Again at the lowest energy of 14 eV we observe very good qualitative agreement, but theory being generally higher than experiment

by a factor of two. The SMC calculation is between 50% and 200% larger than the present calculation at $E_0 = 15$ eV and appears to be definitely too large, although the SMC distribution generally agrees with the measurements. Interestingly, at 17.5 eV the present measurements show marginally better agreement with the SMC result than with the CCC, particularly at small θ .

For the $E(F)^1\Sigma_g^+$ excitation (figure 8) we observe forward scattering and agreement with theory that is very good. In fact at $E_0 = 15$ eV, theory and experiment are in excellent agreement. The CCC calculation shows very large backward scattering that is not observed in the measurements, as this structure is outside the geometric limits of the spectrometer. A future study to experimentally investigate this structure, possibly employing a Magnetic Angle Changer [53] to access the backward scattering region, would be interesting. Again at $E_0 = 14$ eV, the measurement is considerably smaller in magnitude than the CCC result. The SMC result at 15 eV is much flatter than any of the present data, and does not show the backward peak suggested by the CCC results.

For the excitation of the $c^3\Pi_u$ state (figure 5) agreement between theory and experiment is very good at $E_0 = 17.5$, 16 and 15 eV, save for some minor discrepancies. At 17.5 eV the two most forward scattering angles in the present

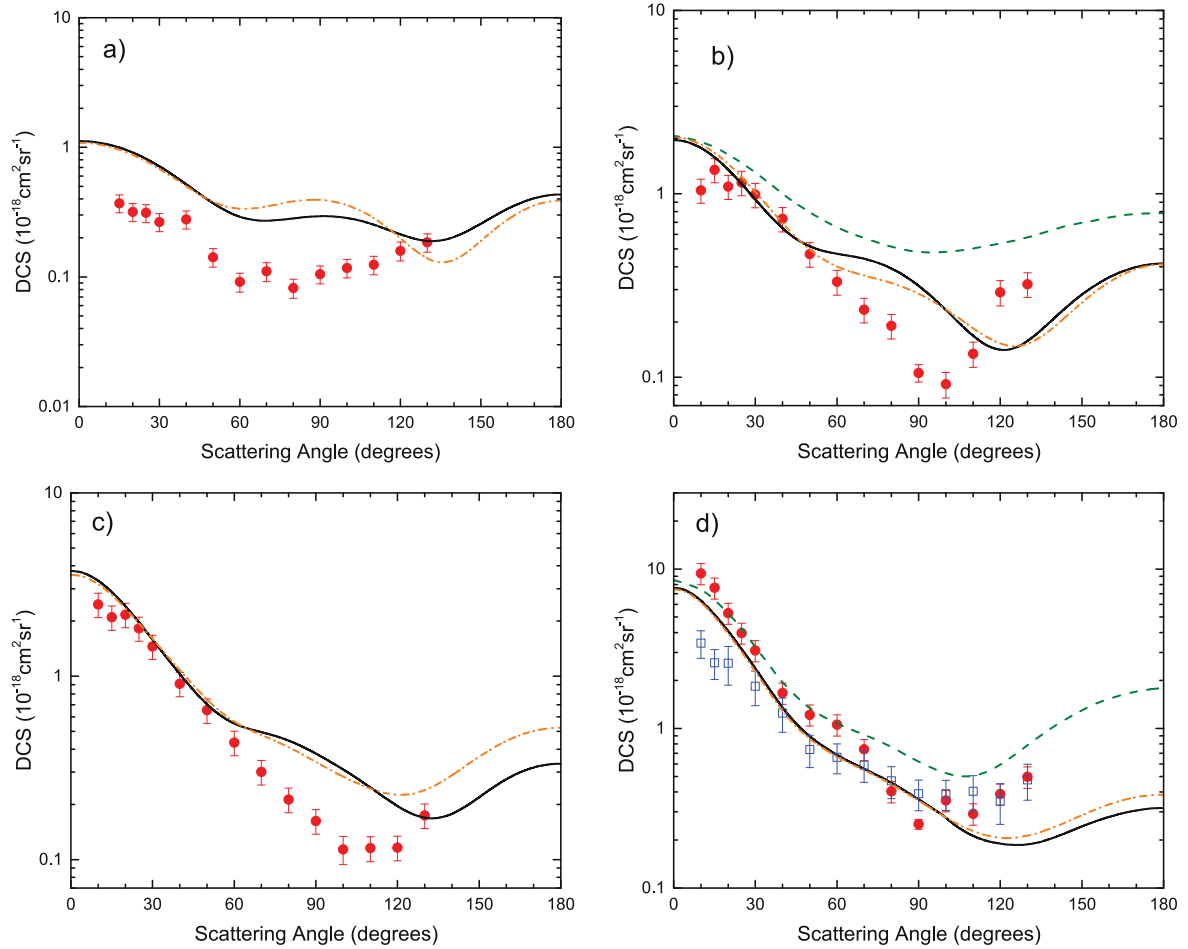


Figure 7. DCS for excitation of the $X^1\Sigma_g^+ \rightarrow C^1\Pi_u$ transition in H_2 at incident energies of (a) 14, (b) 15, (c) 16 and (d) 17.5 eV. Symbols are per figure 4.

measurements rise above the Wrkich *et al* [10] and CCC results. Given the agreement between the measurements of Wrkich *et al* and CCC, plus that the present measured distributions at other energies are all flat we prefer the flatter CCC distribution over the slight forward peak suggested by the current measurements. However, careful repetition and investigation of our unfolding analysis did not reveal any systematic issue in the data analysis. The fact that the discrepancy only presents at a single incident energy is also disconfirmatory of a systematic alignment issue with the apparatus (which would manifest at any energy), and is thus a little puzzling. Even at $E_0 = 14$ eV the angular distributions from the CCC results and experiment are in very good agreement, which shows this state's excitation to be influenced by forward polarizability. The SMC results suggest a much larger forward peak than either the measurements or the CCC results at 17.5 eV and has a qualitatively different shape to either at 15 eV.

For excitation of the $a^3\Sigma_g^+$ state (figure 6), agreement with experiment is very good at $E_0 = 17.5$ eV, again demonstrating polarizability effects at small θ , but agreement is qualitative at the other energies. At the lowest E_0 of 14 eV, the experimental values are smaller than the CCC results by a factor of 3, but the angular distributions agree very well.

Again also, theory shows strong backward scattering which would be interesting to investigate in the future. The present measurements show much improved qualitative agreement with the CCC results compared with the previous measurements of Wrkich *et al* [10], which do not show the minima in the DCS around $\theta = 60^\circ$ and $\theta = 120^\circ$, observed in the present measurements and CCC results at all energies. At 15 eV the SMC results do not predict the DCS as well as the CCC data, missing the small maxima around $\theta = 100^\circ$ seen in both the measurement and the CCC calculation.

In figure 9 we show the DCSs of the above five discussed electronic transitions, summed together at each incident energy. As (perhaps) the most significant challenge for the measurements is to unambiguously unfold the overlapping electronic transition from each other, one way to assess the quality of the unfolded DCSs is to recombine them back together and compare with similarly summed datasets. This procedure mostly removes the unfolding as a factor (albeit higher lying states may continue to play a minor confounding role). At $E_0 = 17.5$ eV we also present the measurements of Wrkich *et al* [10], which have been similarly summed. The present measurements are in excellent agreement with those of Wrkich *et al* at scattering angles greater than 20° . This indicates that there are no basic differences in the two datasets

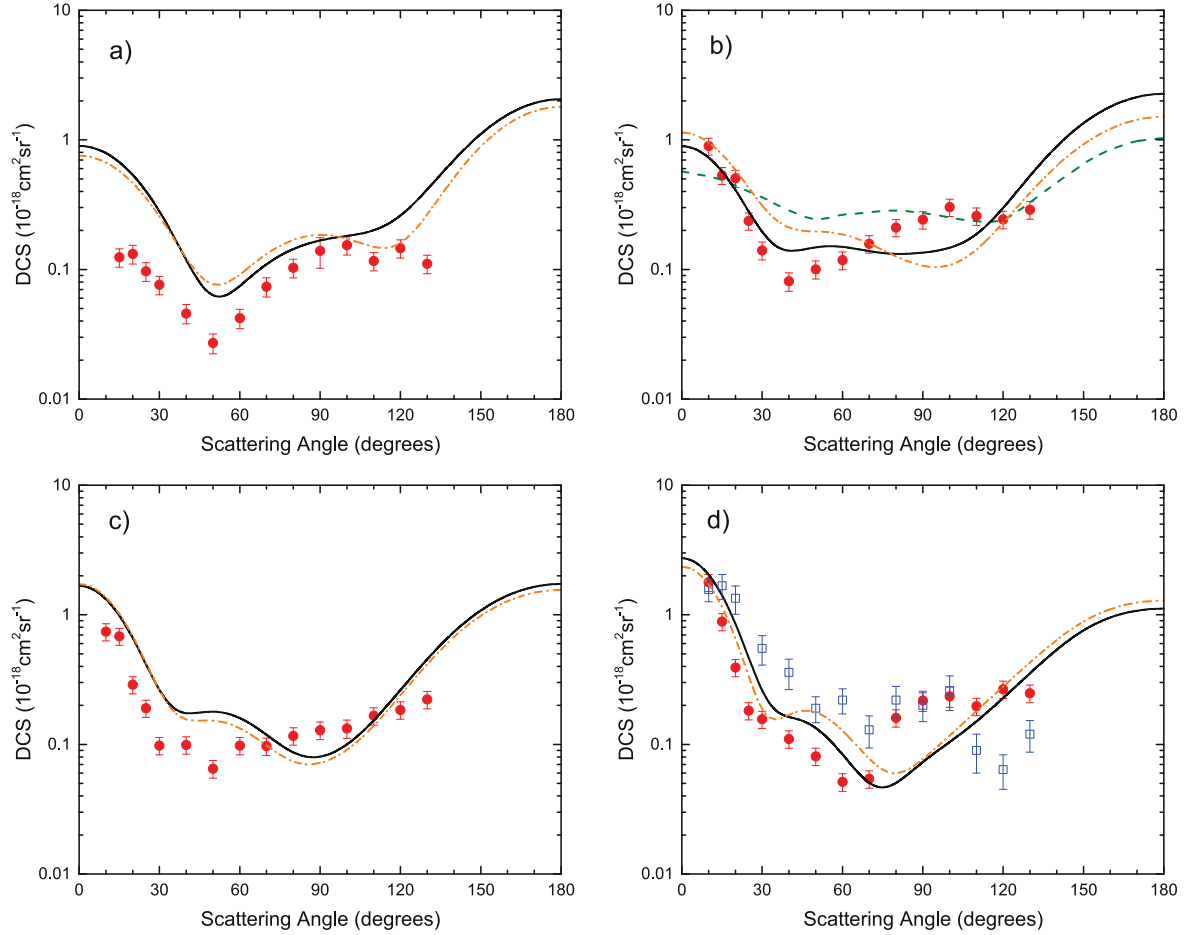


Figure 8. Excitation of the $X\ ^1\Sigma_g^+ \rightarrow E(F)\ ^1\Sigma_g^+$ transition in H_2 at incident energies of (a) 14, (b) 15, (c) 16 and (d) 17.5 eV. Symbols are per figure 4.

for these angles, any differences for the state-resolved DCSs are most likely due to different assumptions in the unfolding. The CCC results are in similarly excellent agreement with both datasets in this angular region. At smaller angles the present measurements exceed the measurements of Wrkich *et al* by as much as a factor of 1.9 (at $\theta = 10^\circ$). The CCC is somewhat in between the two sets of measurements at small angles, the 491-state model is around 30% larger than the data of Wrkich *et al* at 10° , but around 40% smaller than the present measurements at the same angle.

At $E_0 = 16$ and $E_0 = 15$ eV, the present measurements are in excellent agreement with the 427-state CCC model at all scattering angles, and also in excellent agreement with the 491-state model at 16 eV. This observation indicates that differences between the unfolded DCSs and the CCC data may, at least partially, be explained by limitations in the unfolding procedure for the measurements, either due to limitations in the spectroscopic assumptions or non-uniqueness in the fitting. At $E_0 = 14$ eV the summed measurements are smaller than the CCC data at all scattering angles by factor of approximately two, although the angular distribution of the two DCSs remains in excellent agreement. This difference in magnitude cannot be accounted for by the unfolding routine, and so this observation either indicates a problem for the theory at the lowest energy or some unidentified problem with

the normalization of the measurements (or a combination of both). If the latter is the case, this is most likely due to some limitation in the characterization of the analyzer's response function, as the residual energy of the detected electrons is lowest here. If the former, at near-threshold energies the approximation scheme employed by the calculation can be expected to have a significant effect on the cross section, and so an adiabatic nuclei approximation may improve agreement with experiment here.

In figure 10, the present ICS calculations are in very good agreement with experiment for the $B\ ^1\Sigma_u^+$, $c\ ^3\Pi_u$ and $C\ ^1\Pi_u$ excitations, but in poorer agreement with excitation of $a\ ^3\Sigma_g^+$, and $E(F)\ ^1\Sigma_g^+$ states. Note that the CCC data represent an average of the 491- and 427-state models. Also shown are the SMC results and measurements of Wrkich *et al* [10] and Khakoo and Trajmar [8], at energies up to 60 eV. The SMC results show strong resonance structures that are not observed in the CCC results and generally gives higher ICSs. For the $E(F)\ ^1\Sigma_g^+$ excitation ICSs, there seems to be a hint of a resonance at $E_0 = 15$ eV. The CCC results exhibit a very small peak at 15 eV, while the SMC results shows a much more pronounced peak at 14 eV. The 15 eV peak seen in the present measurements may therefore be related to either of these structures.

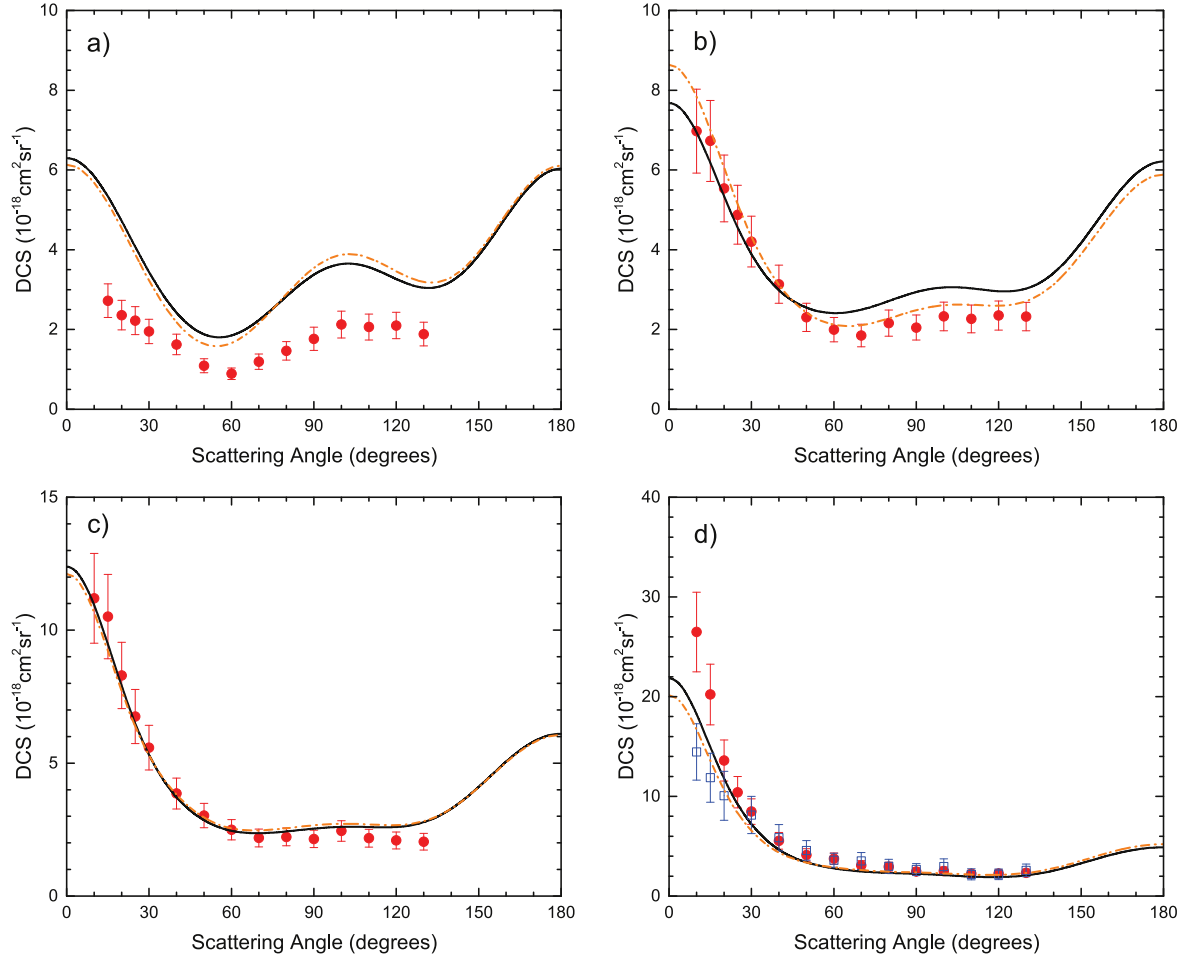


Figure 9. Sum of the 5 lowest electronic transitions in H_2 at incident energies of (a) 14, (b) 15, (c) 16 and (d) 17.5 eV. Symbols are per figure 4.

We also consider the ICS of the sum of the five individual transitions, again to remove the unfolding of the measurements as a factor. The rise from threshold in the summed ICS is shifted to a lower energy in the CCC results compared with the present measurement. The data of Wrkich *et al* and also that of Khakoo and Trajmar follow roughly the same rise as the present measurements up to around 10 eV above threshold, and also show a maximum in the summed ICS at $E_0 = 20$ eV. This maximum is not observed in the CCC data, which suggests a monotonically increasing cross section over the entire energy range. The threshold behavior of the cross sections is likely to be sensitive to the approximation scheme employed in the calculation. A calculation at the adiabatic nuclei approximation level may have a strong effect on the behavior of the ICSs in this energy region, compared with the fixed-nuclei approximation employed here. This is particularly true for the triplet states, whose cross section shows a very rapid rise from threshold compared with the singlet states where the onset is slower, as seen in both the CCC results and the present measurements.

Interestingly, the recent CCC data of Zammit *et al* [51], in particular for the $b^3\Sigma_u^+$ state, also showed a discrepancy with previous experiments in this energy range, with the

measurements becoming progressively larger than the CCC results from around 14–30 eV. The present measurements unfortunately offer no insight into the $b^3\Sigma_u^+$ state as the energy loss range where the state occurs was not scanned in the present study. However, in light of the present data and results of [51], a lower energy resolution study considering the entire EELS from threshold to cutoff, in order to measure a ‘total inelastic’ cross section, would be very interesting.

5. Summary

We present DCSs for excitation of ground vibrational state of H_2 to the lowest five bound electronic states, at E_0 values from 14 to 17.5 eV. The DCSs show predominantly forward scattering due to the polarizability of H_2 . These DCSs are in very good agreement with the present CCC results for E_0 down to 15 eV. At $E_0 = 14$ eV, significant deviation between the experiment and the CCC is observed, with the measurements consistently smaller in magnitude than the CCC results. This is possibly due to the increased presence of nuclear dynamics in the scattering process near threshold, although may also be related to the approximation scheme of the

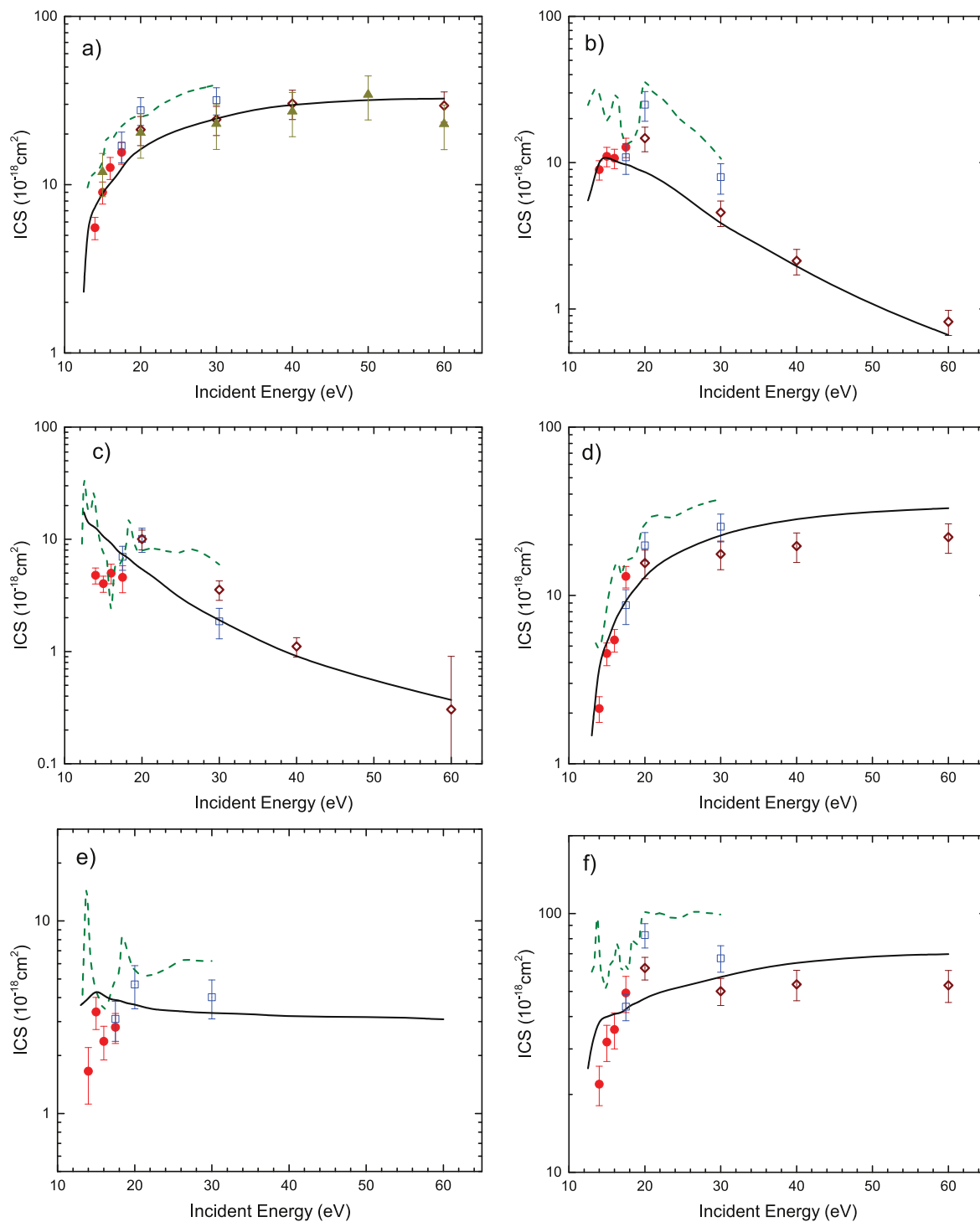


Figure 10. ICS for excitation from the $X\ ^1\Sigma_g^+$ state to the (a) $B\ ^1\Sigma_u^+$, (b) $c\ ^3\Pi_u$, (c) $a\ ^3\Sigma_g^+$, (d) $C\ ^1\Pi_u$ and (e) $E(F)\ ^1\Sigma_g^+$ states of H_2 , and (f) the summed ICS of the previous five states. Symbols are per figure 4, with the addition of the measurements of Khakoo and Trajmar (open maroon diamonds) [8].

calculation or the normalization of the experiment. Given the similar discrepancy between the CCC and measurements for excitation into the first dissociative state observed in previous studies in this energy range, further study into excitation, with a focus on the gross magnitude of the inelastic cross section, between threshold to 30 eV would be very valuable.


Acknowledgments

MAK and LRH acknowledge support from National Science Foundation research grants NSF-RUI-AMO 1306742 and 0968874. XL acknowledges financial support through NASA's Planetary Atmospheres (PATM) and NSF-AST-1518304

program. This work was also supported by the United States Air Force Office of Scientific Research, Los Alamos National Laboratory (LANL) and Curtin University. Zammit would like to specifically acknowledge LANL's ASC PEM Atomic Physics Project for its support. The LANL is operated by Los Alamos National Security, LLC for the National Nuclear Security Administration of the US Department of Energy under Contract No. DEAC52-06NA25396. The authors thank Dr James Colgan (LANL) for reviewing this manuscript

ORCID iDs

L R Hargreaves  <https://orcid.org/0000-0001-5023-6300>

X Liu  <https://orcid.org/0000-0003-2407-316X>

D V Fursa  <https://orcid.org/0000-0002-3951-9016>

I Bray  <https://orcid.org/0000-0001-7554-8044>

References

- [1] Weingartshofer A, Ehrhardt H, Hermann V and Linder F 1970 *Phys. Rev. A* **2** 294
- [2] Trajmar S, Cartwright D, Rice J, Brinkmann R and Kupperman A 1968 *J. Chem. Phys.* **49** 5464
- [3] Hall R and Andric L 1984 *J. Phys. B: At. Mol. Phys.* **17** 1895
- [4] Nishimura H and Danjo A 1986 *J. Phys. Soc. Japan* **55** 3031
- [5] Khakoo M and Trajmar S 1987 *Phys. Rev. A* **35** 2832
- [6] Khakoo M and Segura J 1994 *J. Phys. B: At. Mol. Opt. Phys.* **27** 2355
- [7] Srivastava S and Jensen S 1977 *J. Phys. B: At. Mol. Phys.* **10** 3341
- [8] Khakoo M and Trajmar S 1986 *Phys. Rev. A* **34** 146
- [9] Cartwright D, Chutjian A, Trajmar S and Williams W 1977 *Phys. Rev. A* **16** 1013
- [10] Wrkich J, Mathews D, Kanik I, Trajmar S and Khakoo M 2002 *J. Phys. B: At. Mol. Opt. Phys.* **35** 4695
- [11] Yoon J S, Song M Y, Han J M, Hwang S, Change W S, Lee B and Itikawa Y 2008 *J. Phys. Chem. Ref. Data* **37** 913
- [12] Lindsay B and Mangan M 2003 Photon and electron interactions with atoms, molecules and ions *Numerical Data and Functional Relationships in Science and Technology* (New York: Springer)
- [13] Brunger M and Buckman S 2002 *Phys. Rep.* **357** 215
- [14] Zecca A, Karwasz G and Brusa R 1996 *Riv. Nuovo Cimento* **19** 1
- [15] da Costa R, da Paixao F and Lima M 2005 *J. Phys. B: At. Mol. Opt. Phys.* **38** 4363
- [16] Lima M, Gibson T, McKoy V and Huo W 1988 *Phys. Rev. A* **38** 4527
- [17] Parker S, McCurdy C, Rescigno T and Lengsfeld B 1991 *Phys. Rev. A* **43** 3514
- [18] Gofinkiel J and Tennyson J 2005 *J. Phys. B: At. Mol. Opt. Phys.* **38** 1607
- [19] Trevisan C and Tennyson J 2001 *J. Phys. B: At. Mol. Opt. Phys.* **34** 2935
- [20] Stibbe D and Tennyson J 1997 *Phys. Rev. Lett.* **79** 4116
- [21] Branchett S, Tennyson J and Morgan L 1991 *J. Phys. B: At. Mol. Opt. Phys.* **24** 3479
- [22] Branchett S, Tennyson J and Morgan L 1990 *J. Phys. B: At. Mol. Opt. Phys.* **23** 4625
- [23] Pindzola M, Robicheaux F, Loch S and Colgan J 2006 *Phys. Rev. A* **73** 052706
- [24] Zammit M, Savage J, Fursa D and Bray I 2016 *Phys. Rev. Lett.* **116** 233201
- [25] Kawarai Y, Weber T, Azuma Y, Winstead C, McKoy V and Slaughter D 2014 *Phys. Chem. Lett.* **5** 3854
- [26] Varela K, Hargreaves L, Ralphs K, Khakoo M, Winstead C, McKoy V, Rescigno T and Orel A 2015 *J. Phys. B: At. Mol. Opt. Phys.* **48** 115208
- [27] Ralphs K, Serna G, Hargreaves L, Khakoo M, Winstead C and McKoy V 2013 *J. Phys. B: At. Mol. Opt. Phys.* **46** 125201
- [28] Hughes M, James K, Childers J and Khakoo M 2003 *Meas. Sci. Technol.* **14** 1
- [29] Bro R and Jong S D 1997 *J. Chemometr.* **11** 393
- [30] Muse J, Silva H, Lopes M and Khakoo M 2008 *J. Phys. B: At. Mol. Opt. Phys.* **41** 095203
- [31] LeClair L and Trajmar S 1996 *J. Phys. B: At. Mol. Opt. Phys.* **29** 5543
- [32] Liu X, Shemansky D, Abgrall H, Roueff E, Ahmed S and Ajello J 2003 *J. Phys. B: At. Mol. Opt. Phys.* **36** 173
- [33] Liu X, Shemansky D, Yoshi J, Johnson P, Malone C and Ajello J 2016 *Appl. J. Phys.* **818** 120
- [34] Liu X, Shemansky D, Ahmed S, James G and Ajello J 1998 *J. Geophys. Res.* **103** 739
- [35] Liu X, Shemansky D, Abgrall H, Roueff E, Dziczek D, Hansen D and Ajello J 2002 *Astrophys. J. Suppl. Ser.* **138** 229
- [36] Liu X, Johnson P, Malone C, Young J, Kanik I and Shemansky D 2010 *Appl. J. Phys.* **716** 701
- [37] Orlinkowski T, Staszewska G and Wolniewicz L 1999 *Mol. Phys.* **96** 1445
- [38] Wolniewicz L 1993 *J. Chem. Phys.* **99** 1851
- [39] Staszewska G and Wolniewicz L 1999 *J. Mass. Spectrom.* **198** 416
- [40] Wolniewicz L and Staszewska G 2003 *J. Mass. Spectrom.* **217** 181
- [41] Wolniewicz L and Staszewska G 2003 *J. Mass. Spectrom.* **220** 45
- [42] Liu X, Shemansky D, Johnson P, Malone C, Khakoo M and Kanik I 2012 *J. Phys. B: At. Mol. Opt. Phys.* **45** 015201
- [43] Dabrowski I 1984 *Can. J. Phys.* **62** 1639
- [44] Abgrall H, Roueff E, Launay F, Roncin J Y and Subtil J L 1993 *J. Mol. Spectrosc.* **157** 512
- [45] Abgrall H, Roueff E, Launay F, Roncin J Y and Subtil J L 1993 *Astron. Astrophys. Suppl. Ser.* **101** 273
- [46] Abgrall H, Roueff E, Launay F, Roncin J Y and Subtil J L 1993 *Astron. Astrophys. Suppl. Ser.* **101** 323
- [47] Roncin J Y and Launay F 1994 *Atlas of the Vacuum Ultraviolet Emission Spectrum of Molecular Hydrogen* (Washington, DC: American Chemical Society)
- [48] Crosswhite H 1972 *The Hydrogen Wavelength Tables of Gerhard Heinrich Dieke* (New York: Wiley)
- [49] Wolniewicz L 2007 *Mol. Phys.* **105** 1497
- [50] Zammit M, Fursa D and Bray I 2014 *Phys. Rev. A* **90** 022711
- [51] Zammit M, Savage J, Fursa D and Bray I 2017 *Phys. Rev. A* **95** 022708
- [52] Lane N 1980 *Rev. Mod. Phys.* **52** 29
- [53] Read F and Channing J 1996 *Rev. Sci. Instrum.* **75** 2372
- [54] Abgrall H, Roueff E, Launay F, Roncin Y and Subtil J L 1993 *J. Mol. Spectrosc.* **157** 512
- [55] Borges I and Bielshchowsky C 1999 *Phys. Rev. A* **60** 1226